

Work function tuning in hydrothermally synthesized vanadium-doped MoO₃ and Co₃O₄ mesostructures for energy conversion devices

Pietro Dalle Feste^{1,2#}, Matteo Crisci,^{1,3#} Federico Barbon,¹ Marco Salerno,⁴ Filippo Drago,⁵ Mirko Prato,⁴ Silvia Gross,^{1,2,6*} Teresa Gatti,^{3,7*} Francesco Lamberti^{1,2*}

¹ Department of Chemical Sciences, University of Padova, via Marzolo 1, 35131 Padova, Italy

² Interdepartmental Centre Giorgio Levi Cases for Energy Economics and Technology, University of Padova, via Marzolo 9, 35131 Padova, Italy

³ Institute of Physical Chemistry, Justus Liebig University Giessen, 35390 Giessen, Germany

⁴ Materials Characterization Facility, Italian Institute of Technology, via Morego 30, 16163 Genova, Italy

⁵ Nanochemistry, Italian Institute of Technology, Via Morego 30, 16163 Genova, Italy

⁶ Karlsruher Institut für Technologie (KIT), Institut für Technische Chemie und Polymerchemie (ITCP), Engesserstr. 20, 76131 Karlsruhe, Germany

⁷ Center for Materials Research, Justus Liebig University Giessen, Heinrich Buff Ring 17, 35390 Giessen, Germany

* e-mail: silvia.gross@unipd.it ; teresa.gatti@phys.chemie.uni-giessen.de ; francesco.lamberti@unipd.it

These two authors contributed equally

Abstract

The wide interest in developing green energy technologies stimulates the scientific community to seek, for devices, new substitute material platforms with low environmental impact, ease of production and processing and long-term stability. The synthesis of metal oxide (MO) semiconductors fulfils these requirements and efforts are addressed at optimizing their functional properties, through improvement of charge mobility or energy level alignment. Two MOs have rising perspectives for application in light harvesting devices, mainly for the role of charge selective layers but also as light absorbers, namely MoO₃ (an electron blocking layer) and Co₃O₄ (a small band gap semiconductor). The need to achieve better charge transport has prompted us to attempt doping strategies with vanadium (V) ions that, when combined with oxygen in V₂O₅, produce a high work function MO. We report on subcritical hydrothermal synthesis of V-doped mesostructures of MoO₃ and of Co₃O₄, in which a tight control of the doping is exerted by tuning the relative amounts of reactants. We accomplished a full analytical characterization of these V-doped MOs that unambiguously demonstrates incorporation of the vanadium ions in the MO crystal lattice, as well as effects on the optical properties and work function. We foresee a promising future use of these materials as charge selective materials in energy devices based on multilayer structures.

Keyword

Metal oxide, doping, semiconductor, work function tuning, energy device

Introduction

Transition metal oxides are a multifaceted and diversified class of inorganic materials whose chemico-physical, structural and functional properties encompass a very wide range of different features[1–3]. From the structural point of view, also depending on their stoichiometry, they display very different structures, such as, for instance, (the most common) NaCl, rutile, corundum, fluorite, spinel and cuprite structures. As far as their electric behavior is concerned, it ranges from superconductors (e.g. high-T_c copper oxides), to good metallic conductors (e.g. V₂O₃, ReO₃) through semiconductors (e.g. NiO, ZnO, TiO₂, VO₂) and they can also display interesting magnetic (e.g. Fe₃O₄), and electrochromic (e.g. WO₃) characters.[2,3] From the chemical point of view, their properties span the full range from acidic through amphoteric to basic. These chameleonic features allow these materials to be widely used in commercial products combined to their thermal and chemical stability, ease of processing, and excellent mechanical robustness.

Focusing on the semiconducting materials, there is a flourishing research in optimizing electronic properties of metal oxides in order to fulfill the stringent requirements of next generation clean energy conversion devices such as solar cells.[4]

This is the case, for example, of MoO_3 and Co_3O_4 , that show different electrical properties [5–9] but present one issue: the low mobility of charge carriers. In fact, both oxides are used in photovoltaics for different reasons. First, MoO_3 is a n-type semiconductor; however, due to the high band gap (about 3 eV [10]) and a work function similar to that of Au (5.1 eV or higher depending on conditions in which it is measured [11,12]), it is commonly used as hole transporting material (HTM) and/or as blocking layer for hampering photocharges recombination together with other more conductive HTM. This increases the overall cost of device production in terms of money and time consumption. In addition, the charge mobility that affects the actual conductivity of the material is strongly dependent on the exact stoichiometry: the electron conductivity in MoO_3 is almost zero ($10^{-7} \text{ S cm}^{-1}$), whereas in oxygen-poor MoO_{3-x} species the conductivity can be pushed up of several orders of magnitude, reaching 10^4 S cm^{-1} in pure MoO_2 . [13,14] These results are in agreement with the fact that the atmospheric conditions (mainly either vacuum or ambient) dramatically change the valence/conduction band (VB/CB) values estimation measured with conventional spectroscopic techniques, with a remarkable variation found in the literature that inevitably affects the design of device architectures. On the other hand, the spinel Co_3O_4 shows similar low hole mobility (order of $10^{-5} \text{ S cm}^{-1}$), slightly higher due to the presence of a double electronic direct band gap that allows the oxide to have the proper band gap value (about 1.5 eV) to be directly used as light absorber and HTM in a pn-junction-based next generation all-oxide solar cell.[15–18]

As previously mentioned, the charge conductivity is the bottleneck for real implementation of these oxides in high-performance energy-conversion devices. Two are the main strategies used for improving the conductivity of thin films based on these materials: i) improvement in the quality of the film morphology (i.e. by grain boundaries engineering) and ii) chemical doping[19] of the MO constituting the film with heteroatoms to accomplish instead band engineering. Among the different doping elements, specific transition metal ions such as Mn, Fe, Cu, Co, Cr [20–22] are the most promising ones because of the number of oxidations states available that can in principle tune electronic properties of the host MO. Our choice in this work was addressed towards an aliovalent vanadium (V) substitution, because this metal can be easily oxidized to its pentavalent form in V_2O_5 , a MO that possesses a work function between 6.4 eV and 7 eV[23]). In this way, other MOs that contains V(V) ions as dopants could be likely p-doped, thus improving their charge mobility, as occurred in some examples in literature involving vanadium and MoO_3 [24].

In literature the doping of Co_3O_4 has been previously performed using different elements such as Ru, N, La, Sn, Cu, Li, Ag, V and adopting various synthetic/deposition/processing approaches, like co-precipitation [25], plasma treatment[26], spin coating[27], spray coating[28], dip coating[29], magnetron sputtering [30], thermal decomposition[31], and solvothermal or hydrothermal synthesis[32–35]. This last synthetic methodology is the most valuable among the others because it can be carried out under green conditions (water-based solutions) at low costs (i.e. with simple wet-chemistry laboratory equipment and easy chemical procedures), and typically pursue fast crystallization of materials already under low temperature subcritical conditions. Moreover, it allows a good control over reaction conditions (such as the fine tuning of the dopant concentration), while ensuring high yields. However, only a few syntheses are reported in literature for the preparation of V-doped Co_3O_4 . Magnetron sputtering[30] is instead suitable for direct film deposition, but is not usable to obtain materials to be subsequently processed through solution-based technique. A case of V-doped Co_3O_4 synthesized hydrothermally is reported in the literature for catalytic purposes [35], but the electronic properties are not described, thus remaining hitherto un-characterized. On the other hand, starting from a theoretical analysis that predicts the possibility of balancing the oxygen

vacancies in the lattice,[36] MoO_3 has been doped using both chemical and physical deposition techniques such as CVD[37], sol-gel method [38], solution combusted method[39], magnetron sputtering[40], and also hydrothermal routes [41,42], similarly to Co_3O_4 . Differently from cobalt oxides, this last procedure is widely applied for realizing doped Mo_3O_4 samples with different elements such as Ni [37,39], S [43] and a range of other transition metals [44–46] and in particular vanadium [24].

In this work we describe the subcritical hydrothermal synthesis of V-doped Co_3O_4 micro-wires and MoO_3 micro-lamellae starting from water soluble precursors. We also report on the outcomes obtained by implementing a systematic variation in concentration of the introduced dopants (from 1 to 20 at% with respect to the host oxide), which happen to be significantly different for the two investigated MO host matrices, allowing us to draw preliminary conclusions on the arrangement of the V dopant ions within the two different crystalline lattices. We also show that such a tuning of the doping level in these semiconducting MOs can lead to a parallel tuning of the Fermi level towards the realization of materials with higher work function compared to the undoped analogues, with interesting perspectives for applications in energy-conversion devices.

Results and discussion

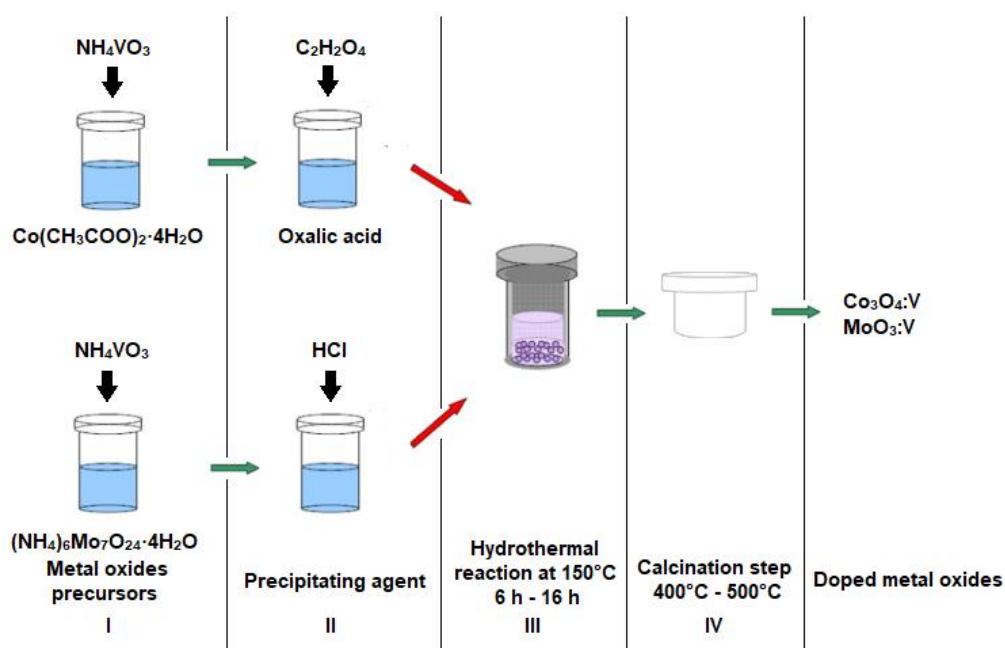


Figure 1. Schematic representation of the hydrothermal synthesis procedure used in this work to obtain the two vanadium-doped MOs, namely $\text{Co}_3\text{O}_4:\text{V}$ and $\text{MoO}_3:\text{V}$.

In Figure 1 a scheme of the hydrothermal synthesis used to prepare V-doped MoO_3 and Co_3O_4 mesostructures is presented (experimental details are provided in the Experimental Section). In the first step, the precursors of cobalt or molybdenum and vanadium are dissolved in water. During the second step, a precipitating agent is added under solution stirring. Next, a Teflon reactor containing the mixture is sealed in a Teflon-lined stainless-steel reactor and heated at 150°C for a set time to perform the hydrothermal reaction in the third step. The separated powders are finally calcined to yield the final V-doped and undoped (for reference) MOs ($\text{Co}_3\text{O}_4:\text{V}$ and $\text{MoO}_3:\text{V}$).

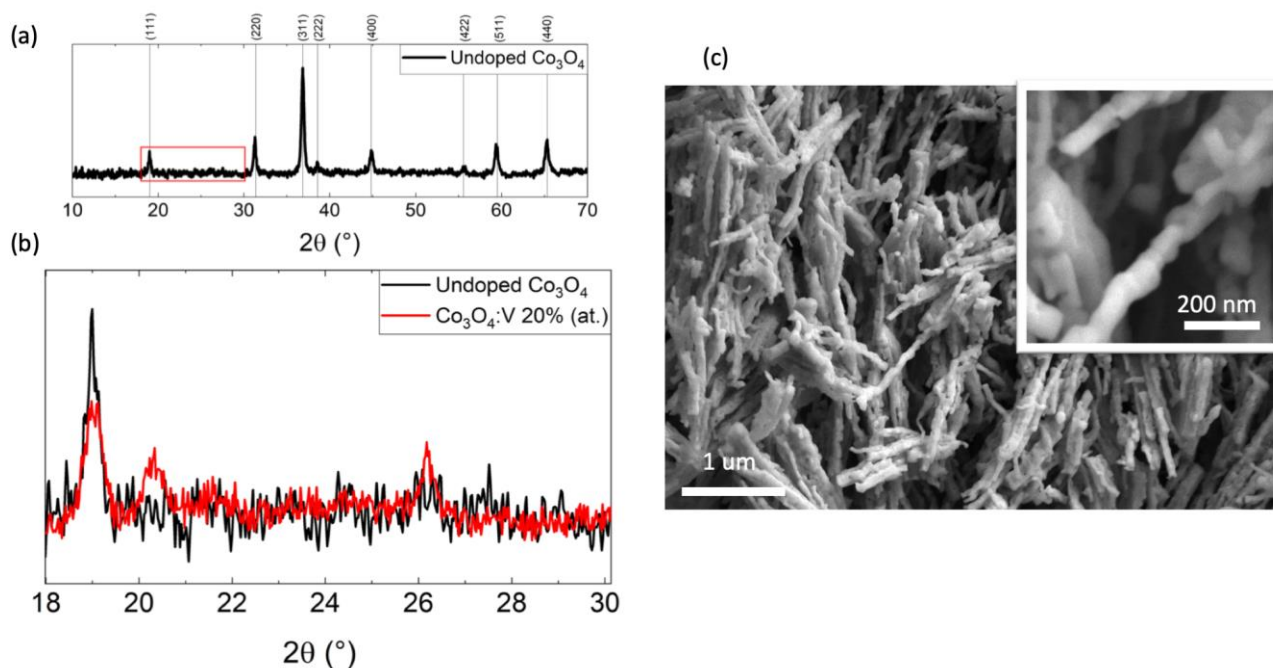


Figure 2. (a) P-XRD diffractogram of hydrothermally synthesized undoped Co_3O_4 . (b) Zoom on the 18° - 30° 2θ range of the same diffractogram and comparison with that of the $\text{Co}_3\text{O}_4:\text{V}$ 20% (at.) sample. (c) SEM image of a typical $\text{Co}_3\text{O}_4:\text{V}$ sample showing the micro-wire-like morphology. The inset shows a magnified area where the particle-like sub-units of the micro-wires are evidenced.

The samples obtained by this procedure are characterized by Powder X-Ray Diffraction (PXRD) to verify the formation of the desired phase (cubic for Co_3O_4 , space group $\text{Fd-}3\text{m}$ (227), alpha for MoO_3 , space group Pbnm (62)). Figure 2a shows the diffractogram of undoped Co_3O_4 (diffractograms of the V-doped samples are reported in the Supporting Information -S.I.- Figure S1), confirming the presence of the cubic Co_3O_4 phase (PDF 74-1657), with a calculated crystalline parameter with Pawley refinement of $a = 8.0838 \pm 0.0014 \text{ \AA}$ (Fig. S3a). The reflections located at $2\theta = 19^\circ, 31.2^\circ, 36.8^\circ, 38.6^\circ, 44.8^\circ, 55.7^\circ, 59.5^\circ$ and 65.3° are attributed to the planes (1 1 1), (2 2 0), (3 1 1), (2 2 2), (4 0 0), (4 2 2), (5 1 1) and (4 4 0) of Co_3O_4 . [47] A signal for V_2O_5 is detected only at the highest nominal concentration of dopant (i.e. 20% at.), as shown in Figure 2b, where weak reflections appear at $2\theta = 20.3^\circ, 26.2^\circ$, which are typical of this MO. Specifically, they are due to the planes (0 0 1), (1 1 0) of crystalline V_2O_5 [48], suggesting the formation of a second MO phase in the synthesized material when a relatively high amount of V-precursor is introduced in the reaction mixture. Topological characterization with scanning electron microscopy (SEM, Figure 2c) discloses the peculiar morphology of this MO, constituted of particles of some tens of nm fused together to generate individual micro-wires.

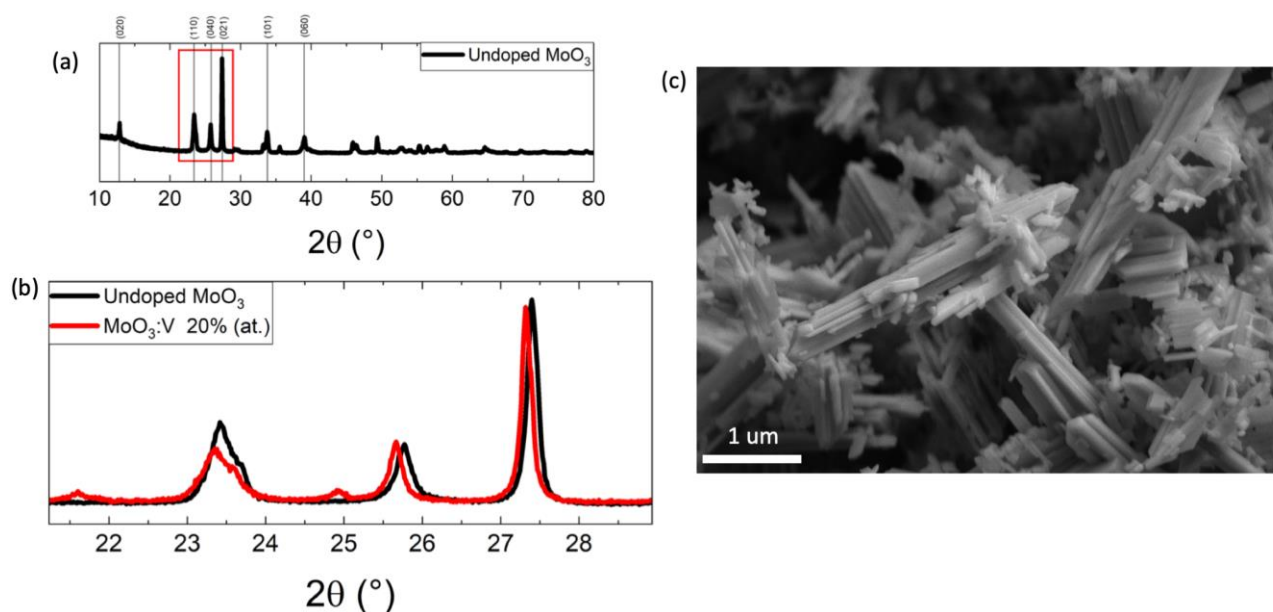


Figure 3. (a) PXRD diffractogram of hydrothermally synthesized undoped MoO_3 . (b) Zoom on the 20.5° - 30° 2θ range of the same diffractogram and comparison with that of the $\text{MoO}_3:\text{V}$ 20% (at.) sample. (c) SEM image of a typical $\text{MoO}_3:\text{V}$ sample showing the micro-lamellar-like morphology.

Figure 3 shows the P-XRD patterns of the undoped MoO_3 and $\text{MoO}_3:\text{V}$ 20% (at.) samples (respectively in Figures 3a and 3b). The reflections correspond to those of the MoO_3 α -phase (PDF 65-2421) with calculated crystalline parameters $a=3.9602\pm 0.0003$ Å, $b=13.8540\pm 0.0011$ Å, $c=3.6949\pm 0.0002$ Å with Pawley refinement (Fig. S3b). However, this analysis shows that a mixture of orthorhombic (α - MoO_3) and monocline (β - MoO_3 , PDF 85-2405) phases of MoO_3 is present in the sample. In addition, major diffraction peaks (with relative planes) corresponding to the desired phase – α - MoO_3 , can be seen at 12.8° , 23.4° , 25.8° , 27.4° , 33.8° , and 39° , relative to the planes (0 2 0), (1 1 0), (0 4 0), (0 2 1), (1 0 1) and (0 6 0), respectively. In Figure 3b two low intensity Bragg peaks at 21.6° and 24.9° are clearly visible, which correspond to a mixed V-Mo oxide phase ($\text{V}_{0.1}\text{Mo}_{0.9}\text{O}_3$ (PDF 81-2414)) [50]. Furthermore, a shift in the Bragg's peaks at 25.8° and 27.4° is found, that can be associated to the partial substitution of V^{5+} in place of Mo^{6+} , as just observed in other MoO_3 doping[51]. For the sake of completeness, the entire set of diffractograms for these MOs is also shown in Figure S1 of the S.I. In addition to the P-XRD diffraction patterns, in Figure 3c a SEM image of a V-doped MoO_3 sample is shown, highlighting the presence of lamellar structures of highly variable dimensions in the order of the μm , similar to what obtained elsewhere in literature[49]: this structural variability can be due to the calcination step, which promotes the coalescence of the smaller objects with the bigger ones, leading to a non-homogenous distribution of size.

The hydrothermally synthesized MO samples have been optically characterized by diffuse reflectance spectroscopy. The recorded spectra are reported in Figure S2 in the S.I. The spectra of $\text{Co}_3\text{O}_4:\text{V}$ samples present two characteristic bands at 700 and 400 nm, attributed to a charge transfer transition from oxygen to the metal centre, namely from O^{2-} to Co^{3+} and from the O^{2-} to Co^{2+} [52]. From the reflectance spectra, a further analysis allows to determine the band gap energy using the Tauc Plot method.[53] This method is based on the relationship existing between light absorbance and band gap energy, described by the equation $(\alpha h\nu)^{1/\gamma} = B(h\nu - E_g)$, [54] where α is the absorption coefficient, $h\nu$ is the incident photon energy, E_g is the energy of the band gap and B is a constant; γ is equal to 1/2 for direct transitions or 2 for indirect ones. In this case, the reflectance spectra are transformed into the corresponding absorption spectra using the Kubelka-Munk Function ($F(R_\infty)$). In the Tauc Plots presented in Figure 4a, the product $(F(R_\infty)h\nu)^{1/\gamma}$ (with γ assuming the value of 1/2

for a direct band gap in Co_3O_4 is plotted as a function of the incident photon energy. The intersection of the linear fit of the Tauc Plot with the x-axis, gives the value of the band gap energy, resulting in two band gaps for the $\text{Co}_3\text{O}_4:\text{V}$ samples.

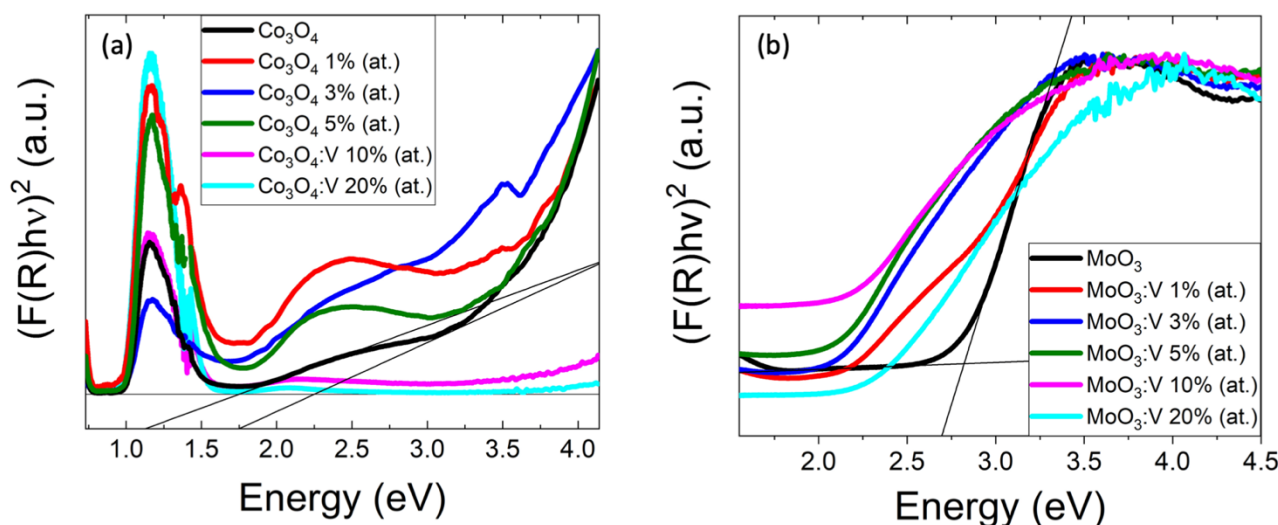


Figure 4. Tauc Plot analysis for the (a) $\text{Co}_3\text{O}_4:\text{V}$ and (b) $\text{MoO}_3:\text{V}$ samples series.

Reflectance measurements and relative band gap calculations were performed for the $\text{MoO}_3:\text{V}$ samples as well (reflectance spectra are reported in Figure S2 of the S.I.). In there, a main band around 470 nm can be observed only for the undoped sample, which shifts towards higher wavelengths for the doped samples, following an unclear relationship with the doping concentration. The Tauc Plot is also built for this second MO series (Figure 4b), with the main difference in the γ value used, 2 in this case for an indirect band gap semiconductor.

The results of all these linear fittings are reported in Table 1. From this analysis, it appears that the bandgap of Co_3O_4 remains almost unvaried, with only a slight increase in the sample doped with 20% (at.) vanadium. For MoO_3 instead a progressive decrease of the E_g from the undoped material is evident, up to the 10% (at.) doped sample, after which a plateau is reached, likely as a consequence of a doping saturation effect.

The shape of the Tauc plots at band gap edges reveals the presence of defects within the band gap of the investigated vanadium-doped cobalt oxides, and a substantial shift of E_g for the vanadium-doped molybdenum ones, suggesting that electronic properties of these MO semiconductors are affected by vanadium inclusion. Therefore, a more detailed electronic characterization is required to understand the effect of the ionic dopant on the energetics of these species, which can be obtained by Kelvin Probe Microscopy (KPM), together with a precise analytical determination of the actual quantity of dopants present in the lattice, which can be obtained by Inductively Coupled Plasma Optical Emission Spectrometry (ICP-OES) analysis.

Although similar synthetic conditions were adopted for both the V-doped MOs, we can state with good approximation that only MoO_3 has been successfully doped, as shown by ICP analysis, whose results are reported in Table 1. More in detail, significantly lower amounts of vanadium are found within the Co_3O_4 -based samples with respect to the MoO_3 -based ones, despite the experimental and nominal doping concentrations being similar. This result is in substantial accordance with the trend in E_g values determined from the Tauc plots, in which the band gap does not change in Co_3O_4 , while it decreases with increasing doping in MoO_3 , for at least the first three samples (see Figure 4 and Table 1). Furthermore, the ICP analysis highlights that a significant amount of dopant is found already at very low V concentrations in MoO_3 , suggesting that a substitutional doping might occur

and that the inclusion of vanadium ions can be tuned acting on the stoichiometry of the reactants. On the contrary, the Co_3O_4 samples do not show any relevant vanadium incorporation except for the 20% (at.) specimen, which most likely is a biphasic material, i.e. a mixed V_2O_5 - Co_3O_4 composite, as anticipated from P-XRD (Figure 2b). The reason for this different doping behavior with respect to the vanadium ion dopants can probably be ascribed to the different crystal structures of the MOs - with α - MoO_3 and V_2O_5 being both orthorhombic whereas Co_3O_4 having a cubic lattice. In light of these considerations, it appears reasonable to foresee an easier accommodation of the V(V) cations in the structure of MoO_3 with respect to that of Co_3O_4 . On the other hand, we exclude a pure influence of the ionic radii of the cations on the doping efficiency, because these are comparable for all the cations here considered, with the same coordination number (65/54 pm for Co (II/III), 59 pm for Mo(VI) and 54 pm for V(V)).[55]

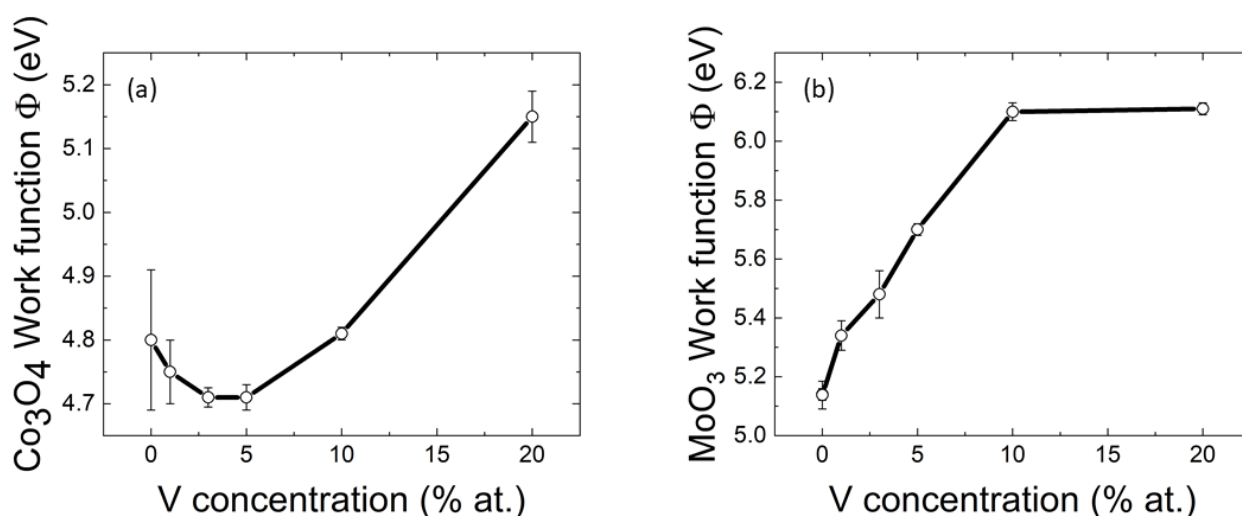


Figure 5. Work function values estimated through Kelvin probe microscopy analysis for the (a) Co_3O_4 :V and (b) MoO_3 :V samples series.

KPM analysis provides a value of the work function (WF), which can substantially vary upon effective chemical doping, and thus provides information on the doping character (p- or n-) in the semiconducting materials. The trends in WF of the MO materials (Figure 5) are highly related to the optical and ICP data: in the Co_3O_4 :V samples series the WF remains practically unchanged (4.7÷4.8 eV) across most doping values except for the highest one, for which a significant variation takes place (from ~4.75 eV up to ~5.15 eV). The increased WF being obtained only at the highest V-doping level in Co_3O_4 can be related to the presence of the second V_2O_5 phase formed, which is perhaps located on the external surface of the MO mesostructures, thus largely contributing to the measured value (WF of pure V_2O_5 should be ~7 eV [56]). On the contrary, for the MoO_3 samples, a linear increase of the WF (from 5.14 eV to 6.10 eV) is observed with increasing dopant concentration, for the lowest values thereof, while the WF does not increase further only at the highest concentration (with a 6.11 eV WF value obtained when the actual amount of vanadium in the MO doubles from 10 at% to 20 at%), thus suggesting also in this case the occurrence of a phase separation within the material as for the case of Co_3O_4 :V 20 at%. These results (with nominal doping concentrations corroborated by ICP data), suggest that only in the case of MoO_3 an hypothetical substitutional p-doping of the material is obtained by using the hydrothermal method, whereas for Co_3O_4 any additional determined p-character can be only attributed to the presence of a V_2O_5 phase formed in conjunction. However, an interesting two-phase composite material appear, with high crystalline content as revealed by P-XRD, which possesses the characteristics of both the constituents (the E_g of pristine Co_3O_4 and a deeply located Fermi level similar to V_2O_5), what could be useful for photovoltaic applications.

Table 1. Summary of chemical and electrical properties for the series of hydrothermally synthesized undoped and V-doped Co_3O_4 and MoO_3 samples investigated in the present study.

Sample	V % ¹	E_g (eV) ² ($\pm 4\%$)	WF (eV) ⁴
Undoped Co_3O_4	-	1.74; 2.24 ³	4.8 ± 0.11
Co_3O_4 :V (1% at)	< 1	1.50; 2.20 ³	4.75 ± 0.05
Co_3O_4 :V (3% at)	< 1	1.50; 2.20 ³	4.71 ± 0.02
Co_3O_4 :V (5% at)	< 1	1.65; 2.14 ³	4.71 ± 0.02
Co_3O_4 :V (10% at)	< 1	1.48; 2.35 ³	4.81 ± 0.01
Co_3O_4 :V (20% at)	12	1.63; 2.62 ³	5.15 ± 0.04
Undoped MoO_3	-	2.8	5.14 ± 0.05
MoO_3 (1% at)	1	2.3	5.34 ± 0.05
MoO_3 (3% at)	3	2.1	5.48 ± 0.08
MoO_3 (5% at)	4	2.1	5.70 ± 0.02
MoO_3 (10% at)	6	2.2	6.10 ± 0.03
MoO_3 (20% at)	13	2.3	6.11 ± 0.02

¹ Actual vanadium atomic concentration as determined by ICP analysis and calculated as: V % = number of V dopant atoms/100 host metal atoms (namely, Mo or Co); ² E_g extracted from Tauc plot analysis with a $\pm 4\%$ associated error; ³ For Co_3O_4 two E_g values are extracted; ⁴ Determined by KPM analysis.

Conclusions

In this work we demonstrated the efficient incorporation of V ions in a MoO_3 scaffold until a relatively high atomic percentage (10%), resorting to a green hydrothermal method that starts from polyoxometalate and carboxylate precursors. We also showed the effect of such an incorporation on

the work function of the MO semiconducting scaffold, which results in a progressive (and almost linear) increase (with respect to the vacuum level), thus allowing us to predict an effective p-doping of the material that enables tuning of the charge transport properties of the materials, whose actual determination remains the subject of future work. In addition, it should be pointed out that the nature of the Mo(VI) substitution with aliovalent extrinsic V(V) cations in the lattice is only hypothesized at the moment, and its confirmation would be obtained through X-ray absorption spectroscopy investigations performed at synchrotron, which is a suitable method to investigate the typology of ion incorporation into doped materials.

On the other hand, we showed that a low band gap Co_3O_4 MO semiconductor (also prepared through hydrothermal synthesis) cannot guest V ions into its lattice, although V(V) and Co(II/III) ionic radii are quite similar in dimension, and the modulation of the WF is achievable only when a relatively high concentration of vanadium precursor is added, thus forming a 2-phases compound based on V_2O_5 and Co_3O_4 . Although the synthetic goal of this work was mainly demonstrating the possibility of substitutional (or even interstitial) doping of the two considered MO matrices, we will next characterize this Co-V composite further, to better understand its structural features and evaluate its real potential for application in sustainable technologies for conversion of light energy into other useful forms (electricity, solar fuels, but even into light energy storage applications, given the relevance of cobalt oxides in battery-like devices).

Experimental section

All reagents and solvents were purchased from Sigma Aldrich, if not otherwise specified, and used as received. Powder X-Ray Diffraction was carried out on a Bruker D8 Advance Plus diffractometer using the Cu K_α radiation. Patterns for Co_3O_4 -based samples were recorded in the range $10\text{-}70^\circ$ with a 0.027° (2Θ) scan step and 0.7 s per step acquisition time. For the $\text{Co}_3\text{O}_4\text{:V}$ 20% (at.) sample, one additional XRD pattern was recorded in the range $18\text{-}40^\circ$ with a 0.027° (2Θ) scan step and 2 s per step acquisition time. The XRD patterns of the MoO_3 -based samples were collected with the same instrument in the range $10\text{-}80^\circ$ with a 0.014° (2Θ) scan step and 0.3 s acquisition time per step.

Scanning electron microscopy images were recorded with a Zeiss SUPRA 35VP instrument.

UV-Visible reflectance spectra were acquired on a Cary 5000 spectrophotometer equipped with an integrating sphere.

Kelvin probe microscopy measurements on hydrothermally synthesized MO powders were carried out in ambient air with an atomic force microscope MFP-3D by Asylum Research (Oxford Instruments, UK). A probe ASYELEC.02 was used, with nominal cantilever resonance frequency of 300 kHz, and tip coated with 25 nm thick Ti/Ir film. The scan was two-pass, with surface potential measured during the second pass at elevated height (typically 80 nm). The WF of the tip was first determined, by measuring the electrical surface potential V on highly-oriented pyrolytic graphite (HOPG), whose work function was assumed to be 4.6 eV. Measurements were carried out on a thick (bulk) layer of sample powder, pressed to form a solid pellet, finding consistent values, within the estimated uncertainty (± 100 mV). The obtained value resulted from averaging the means from $N=4$ images of typical $5\ \mu\text{m}$ scan size, in different sample locations.

Elemental analysis was carried out via Inductively Couple Plasma Optical Emission Spectrometry (ICP-OES), with an iCAP 7600 DUO (Thermo Fisher Scientific). Samples were weighted and digested in a single overnight step, in the case of Co_3O_4 -based samples, in a flask with aqua regia; MoO_3 -based samples were instead digested in a two-step process, first with HF and then with aqua regia. The digested samples were diluted to 10 mL using ultrapure Milli-Q water and filtered using a $0.45\ \mu\text{m}$ PTFE filter before the analysis. ICP-OES was used to determine the relative amount of vanadium with respect to the metal in the MO sample. Values were evaluated using the Qtegra software (ThermoFisher).

Hydrothermal synthesis of V-doped Co_3O_4 and V-doped MoO_3 .

For a typical hydrothermal synthesis of V-doped Co_3O_4 and V-doped MoO_3 , adapting procedures reported in literature[35,57], a given amount of metal precursor are dissolved in deionized water (10 mL). The precursor is either 0.15 M cobalt acetate tetrahydrate (Carlo Erba, City, Country) or 0.05 M ammonium eptamolybdate tetrahydrate (Alfa Aesar, City, Country) and ammonium metavanadate, in order to have in the mixture different atomic ratios between cobalt or molybdate precursor and vanadium (V: 1%, 3%, 5%, 10%, 20% at.). At the cobalt precursor solution, oxalic acid with a molar ratio 1:1 with respect to cobalt acetate is added, following by stirring for 30 min. The molybdenum precursor solution is instead stirred for 20 min, then 275 μL of HCl 37% v/v are added, and next the solution is stirred for other 20 min. Each solution is prepared in a A255AC PTFE cup (Parr Instrument Company). After the dissolution of the reagents, the PTFE cup is placed in a stainless steel 4745 General Purpose Acid-Digestion Bomb (Parr Instrument Company) and heated at 150 °C for 6 h (Co_3O_4 synthesis) or 16 h (MoO_3 synthesis). After the reaction, the autoclave is allowed to cool down at room temperature. The resulting solid powder is isolated by centrifugation, washed twice with deionized water and once with absolute ethanol, and dried in an oven at 80 °C. Finally, the powder is calcinated in a muffle at 400°C for 2 h (Co_3O_4 synthesis) or at 500°C for 3 h (MoO_3 synthesis), to convert it to the desired crystalline phase.

Author contributions

Conceptualization, S.G., T.G. and F.L.; methodology, S.G., T.G. and F.L.; validation, S.G., T.G. and F.L.; formal analysis, T.G. and F.L.; investigation, M.C., P.D.F., F.B., F.D., M.S., M.P., S.G., T.G. and F.L.; resources, M.S., M.P., S.G., T.G. and F.L.; data curation, T.G. and F.L.; writing—original draft preparation, M.C., P.D.F, T.G. and F.L.; writing-review and editing F.B., S.G., T.G. and F.L.; visualization, F.L. and T.G.; supervision, S.G., T.G. and F.L.; project administration, S.G., T.G. and F.L.; funding acquisition, S.G., T.G. and F.L. All authors have read and agreed to the published version of the manuscript.

Fundings

P.D.F., S.G. and F.L. acknowledge financial support from the Interdepartmental Centre Giorgio Levi Cases for Energy Economics and Technology of the University of Padova with the project AMON-RA. S.G. thanks the Department of Excellence Project “NEXUS” for providing equipment and spaces. T.G. and M. C. thank the European Commission for the H2020 FET-PROACTIVE-EIC-07-2020 project LIGHT-CAP (project number 101017821) and the Verband der Chemischen Industrie e.V. for the “Fonds der Chemischen Industrie”. Francesca Tajoli (DiSC, University of Padova) is gratefully acknowledged for performing all P-XRD and SEM analyses.

Conflicts of Interest

The authors declare no conflict of interest.

References

- [1] Cox PA. Transition Metal Oxides: An Introduction to Their Electronic Structure and Properties. OUP Oxford; 2010.
- [2] Rao CNR, Raveau B. Transition Metal Oxides: Structure, Properties, and Synthesis of Ceramic Oxides, 2nd Edition. 2nd ed. Weinheim: Wiley VCH; 1998.
- [3] Greenwood NN, Earnshaw A. Chemistry of the Elements. Elsevier; 1997.
- [4] Pérez-Tomás A, Mingorance A, Tanenbaum D, Lira-Cantú M. Chapter 8 - Metal Oxides in

Photovoltaics: All-Oxide, Ferroic, and Perovskite Solar Cells. In: Lira-Cantu MBT-TF of SO in N-GSC, editor. *Met. Oxides*, Elsevier; 2018, p. 267–356. doi:<https://doi.org/10.1016/B978-0-12-811165-9.00008-9>.

- [5] Girardi L, Bardini L, Michieli N, Kalinic B, Maurizio C, Rizzi G, et al. Co₃O₄ Nanopetals on Si as Photoanodes for the Oxidation of Organics. *Surfaces* 2019;2:41–53. doi:10.3390/surfaces2010004.
- [6] Kim J, Iivonen T, Hämäläinen J, Kemell M, Meinander K, Mizohata K, et al. Low-Temperature Atomic Layer Deposition of Cobalt Oxide as an Effective Catalyst for Photoelectrochemical Water-Splitting Devices. *Chem Mater* 2017;29:5796–805. doi:10.1021/acs.chemmater.6b05346.
- [7] Mai L, Yang F, Zhao Y, Xu X, Xu L, Hu B, et al. Molybdenum oxide nanowires: synthesis & properties. *Mater Today* 2011;14:346–53. doi:10.1016/S1369-7021(11)70165-1.
- [8] Haber J, Lalik E. Catalytic properties of MoO₃ revisited. *Catal Today* 1997;33:119–37. doi:10.1016/S0920-5861(96)00107-1.
- [9] Mane AA, Nikam SA, Moholkar AV. NO₂ gas sensing properties of sprayed composite porous MoO₃-V₂O₅ thin films. *Mater Chem Phys* 2018;216:294–304. doi:10.1016/j.matchemphys.2018.05.043.
- [10] Bhatia S, Khanna A. Structural and optical properties of molybdenum trioxide thin films, 2015, p. 080057. doi:10.1063/1.4917961.
- [11] Guo Y, Robertson J. Origin of the high work function and high conductivity of MoO₃. *Appl Phys Lett* 2014;105:222110. doi:10.1063/1.4903538.
- [12] Tao C, Ruan S, Zhang X, Xie G, Shen L, Kong X, et al. Performance improvement of inverted polymer solar cells with different top electrodes by introducing a MoO₃ buffer layer. *Appl Phys Lett* 2008;93:193307. doi:10.1063/1.3026741.
- [13] De Melo O, Torres-Costa V, Climent-Font A, Galán P, Ruediger A, Sánchez M, et al. Optical and electrical properties of MoO₂ and MoO₃ thin films prepared from the chemically driven isothermal close space vapor transport technique. *J Phys Condens Matter* 2019;31. doi:10.1088/1361-648X/ab18e2.
- [14] Prasad AK, Gouma PI, Kubinski DJ, Visser JH, Soltis RE, Schmitz PJ. Reactively sputtered MoO₃ films for ammonia sensing. *Thin Solid Films* 2003;436:46–51. doi:10.1016/S0040-6090(03)00524-8.
- [15] Kupfer B, Majhi K, Keller DA, Bouhadana Y, Rühle S, Barad HN, et al. Thin Film Co₃O₄/TiO₂ Heterojunction Solar Cells. *Adv Energy Mater* 2015;5:1401007. doi:10.1002/aenm.201401007.
- [16] Rühle S, Anderson AY, Barad H-N, Kupfer B, Bouhadana Y, Rosh-Hodesh E, et al. All-Oxide Photovoltaics. *J Phys Chem Lett* 2012;3:3755–64. doi:10.1021/jz3017039.
- [17] Zhou Y, Zhang X, Lu X, Gao X, Gao J, Shui L, et al. Promoting the Hole Extraction with Co₃O₄ Nanomaterials for Efficient Carbon-Based CsPbI₂Br Perovskite Solar Cells. *Sol RRL*

2019;3:1800315. doi:10.1002/solr.201800315.

- [18] Bashir A, Shukla S, Lew JH, Shukla S, Bruno A, Gupta D, et al. Spinel Co₃O₄ nanomaterials for efficient and stable large area carbon-based printed perovskite solar cells. *Nanoscale* 2018;10:2341–50. doi:10.1039/C7NR08289D.
- [19] Righetto M, Meggiolaro D, Rizzo A, Sorrentino R, He Z, Meneghesso G, et al. Coupling halide perovskites with different materials: From doping to nanocomposites, beyond photovoltaics. *Prog Mater Sci* 2020;110:100639. doi:https://doi.org/10.1016/j.pmatsci.2020.100639.
- [20] Yuhas BD, Zitoun DO, Pauzuskie PJ, He R, Yang P. Transition-Metal Doped Zinc Oxide Nanowires. *Angew Chemie Int Ed* 2006;45:420–3. doi:10.1002/anie.200503172.
- [21] Jansons AW, Koskela KM, Crockett BM, Hutchison JE. Transition Metal-Doped Metal Oxide Nanocrystals: Efficient Substitutional Doping through a Continuous Growth Process. *Chem Mater* 2017;29:8167–76. doi:10.1021/acs.chemmater.7b02176.
- [22] Stavale F, Shao X, Nilus N, Freund H-J, Prada S, Giordano L, et al. Donor Characteristics of Transition-Metal-Doped Oxides: Cr-Doped MgO versus Mo-Doped CaO. *J Am Chem Soc* 2012;134:11380–3. doi:10.1021/ja304497n.
- [23] Hermann K, Witko M, Druzinic R, Chakrabarti A, Tepper B, Elsner M, et al. Properties and identification of oxygen sites at the V₂O₅(010) surface: Theoretical cluster studies and photoemission experiments. *J Electron Spectros Relat Phenomena* 1999;98–99:245–56. doi:10.1016/s0368-2048(98)00290-4.
- [24] Qu G, Wang J, Liu G, Tian B, Su C, Chen Z, et al. Vanadium Doping Enhanced Electrochemical Performance of Molybdenum Oxide in Lithium-Ion Batteries. *Adv Funct Mater* 2019;29:1805227. doi:10.1002/adfm.201805227.
- [25] Singh PK, Singh N, Singh M, Tandon P, Singh SK. Preparation of Nanostructured Co₃O₄ and Ru-Doped Co₃O₄ and Their Applicability in Liquefied Petroleum Gas Sensing. *J Mater Eng Perform* 2019;28:7592–601. doi:10.1007/s11665-019-04495-0.
- [26] Xu L, Wang Z, Wang J, Xiao Z, Huang X, Liu Z, et al. N-doped nanoporous Co₃O₄ nanosheets with oxygen vacancies as oxygen evolving electrocatalysts. *Nanotechnology* 2017;28:165402. doi:10.1088/1361-6528/aa6381.
- [27] Shaban M, El Sayed AM. Influence of the spin deposition parameters and La/Sn double doping on the structural, optical, and photoelectrocatalytic properties of CoCo₂O₄ photoelectrodes. *Sol Energy Mater Sol Cells* 2020;217:110705. doi:10.1016/j.solmat.2020.110705.
- [28] Venkatesh R, Dhas CR, Sivakumar R, Dhandayuthapani T, Subramanian B, Sanjeeviraja C, et al. Tailoring the physical properties and electrochromic performance of nebulizer spray coated Co₃O₄ films through copper doping. *Solid State Ionics* 2019;334:5–13. doi:10.1016/j.ssi.2019.01.029.
- [29] Švegl F, Orel B, Grabec-Švegl I, Kaučič V. Characterization of spinel Co₃O₄ and Li-doped

Co₃O₄ thin film electrocatalysts prepared by the sol–gel route. *Electrochim Acta* 2000;45:4359–71. doi:10.1016/S0013-4686(00)00543-0.

- [30] Xing Z, Wu H, Wu L, Wang X, Zhong H, Li F, et al. A multifunctional vanadium-doped cobalt oxide layer on silicon photoanodes for efficient and stable photoelectrochemical water oxidation. *J Mater Chem A* 2018;6:21167–77. doi:10.1039/C8TA07552B.
- [31] El-Shobaky GA, Turkey AE-MM. Catalytic decomposition of H₂O₂ on Co₃O₄ doped with MgO and V₂O₅. *Colloids Surfaces A Physicochem Eng Asp* 2000;170:161–72. doi:10.1016/S0927-7757(00)00496-9.
- [32] Ali F, Khalid NR. Effect of calcination temperature on structural, morphological and electrochemical properties of Sn doped Co₃O₄ nanorods. *Ceram Int* 2020;46:24137–46. doi:10.1016/j.ceramint.2020.06.193.
- [33] Aadil M, Zulfiqar S, Shahid M, Haider S, Shakir I, Warsi MF. Binder free mesoporous Ag-doped Co₃O₄ nanosheets with outstanding cyclic stability and rate capability for advanced supercapacitor applications. *J Alloys Compd* 2020;844:156062. doi:10.1016/j.jallcom.2020.156062.
- [34] Jiang T, Yin N, Bai Z, Dai P, Yu X, Wu M, et al. Wet chemical synthesis of S doped Co₃O₄ nanosheets/reduced graphene oxide and their application in dye sensitized solar cells. *Appl Surf Sci* 2018;450:219–27. doi:10.1016/j.apsusc.2018.04.148.
- [35] Wei R, Bu X, Gao W, Villaos RAB, Macam G, Huang Z-Q, et al. Engineering Surface Structure of Spinel Oxides via High-Valent Vanadium Doping for Remarkably Enhanced Electrocatalytic Oxygen Evolution Reaction. *ACS Appl Mater Interfaces* 2019;11:33012–21. doi:10.1021/acsami.9b10868.
- [36] Peelaers H, Chabinyo ML, Van de Walle CG. Controlling n-Type Doping in MoO₃. *Chem Mater* 2017;29:2563–7. doi:10.1021/acs.chemmater.6b04479.
- [37] Patil MK, Gaikwad SH, Mukherjee SP. Phase- and Morphology-Controlled Synthesis of Tunable Plasmonic MoO_{3-x} Nanomaterials for Ultrasensitive Surface-Enhanced Raman Spectroscopy Detection. *J Phys Chem C* 2020;124:21082–93. doi:10.1021/acs.jpcc.0c06004.
- [38] Shen J, Guo S, Chen C, Sun L, Wen S, Chen Y, et al. Synthesis of Ni-doped A-MoO₃ nanolamella and their improved gas sensing properties. *Sensors Actuators, B Chem* 2017;252:757–63. doi:10.1016/j.snb.2017.06.040.
- [39] Rammal MB, Omanovic S. Synthesis and characterization of NiO, MoO₃, and NiMoO₄ nanostructures through a green, facile method and their potential use as electrocatalysts for water splitting. *Mater Chem Phys* 2020;255:123570. doi:10.1016/j.matchemphys.2020.123570.
- [40] Ahmad H, Afzal N, Rafique M, Ahmed AA, Ahmad R, Khaliq Z. Post-deposition annealed MoO₃ film based high performance MSM UV photodetector fabricated on Si (100). *Ceram Int* 2020;46:20477–87. doi:10.1016/j.ceramint.2020.05.150.
- [41] Phuruangrat A, Chen JS, Lou XW, Yayapao O, Thongtem S, Thongtem T. Hydrothermal

synthesis and electrochemical properties of α -MoO₃ nanobelts used as cathode materials for Li-ion batteries. *Appl Phys A Mater Sci Process* 2012;107:249–54. doi:10.1007/s00339-012-6771-3.

- [42] Yang X, Ding H, Zhang D, Yan X, Lu C, Qin J, et al. Hydrothermal synthesis of MoO₃ nanobelt-graphene composites. *Cryst Res Technol* 2011;46:1195–201. doi:10.1002/crat.201100302.
- [43] Qin P, Fang G, Cheng F, Ke W, Lei H, Wang H, et al. Sulfur-doped molybdenum oxide anode interface layer for organic solar cell application. *ACS Appl Mater Interfaces* 2014;6:2963–73. doi:10.1021/am405571a.
- [44] Layegh M, Ghodsi FE, Hadipour H. Experimental and theoretical study of Fe doping as a modifying factor in electrochemical behavior of mixed-phase molybdenum oxide thin films. *Appl Phys A Mater Sci Process* 2020;126. doi:10.1007/s00339-019-3188-2.
- [45] Li Z, Wang W, Zhao Z, Liu X, Song P. Facile synthesis and enhanced trimethylamine sensing performances of W-doped MoO₃ nanobelts. *Mater Sci Semicond Process* 2017;66:33–8. doi:10.1016/j.mssp.2017.04.002.
- [46] Cheyng D, Kam B, Vasseur K, Heremans P, Rand BP. Structure induced conductivity enhancement in metal-doped molybdenum oxide thin films. *J Appl Phys* 2013;113:043109. doi:10.1063/1.4789352.
- [47] Deori K, Deka S. Morphology oriented surfactant dependent CoO and reaction time dependent Co₃O₄ nanocrystals from single synthesis method and their optical and magnetic properties. *CrystEngComm* 2013;15:8465. doi:10.1039/c3ce41502c.
- [48] Vijayakumar Y, Mani GK, Reddy MVR, Rayappan JBB. Nanostructured flower like V₂O₅ thin films and its room temperature sensing characteristics. *Ceram Int* 2015;41:2221–7. doi:10.1016/j.ceramint.2014.10.023.
- [49] Chiang T, Yeh H. The Synthesis of α -MoO₃ by Ethylene Glycol. *Materials (Basel)* 2013;6:4609–25. doi:10.3390/ma6104609.
- [50] Rasteiro LF, Vieira LH, Possato LG, Pulcinelli SH, Santilli C V, Martins L. Hydrothermal synthesis of Mo-V mixed oxides possessing several crystalline phases and their performance in the catalytic oxydehydration of glycerol to acrylic acid. *Catal Today* 2017;296:10–8. doi:10.1016/j.cattod.2017.04.006.
- [51] Phuruangrat A, Thongtem S, Thongtem T. Hydrothermal synthesis, characterization, and photocatalytic performance of W-doped MoO₃ nanobelts. *Res Chem Intermed* 2016;42:7487–99. doi:10.1007/s11164-016-2548-1.
- [52] Barreca D, Massignan C, Daolio S, Fabrizio M, Piccirillo C, Armelao L, et al. Composition and Microstructure of Cobalt Oxide Thin Films Obtained from a Novel Cobalt(II) Precursor by Chemical Vapor Deposition. *Chem Mater* 2001;13:588–93. doi:10.1021/cm001041x.
- [53] Kim M, Alfano A, Perotto G, Serri M, Dengo N, Mezzetti A, et al. Moisture resistance in perovskite solar cells attributed to a water-splitting layer. *Commun Mater* 2021;2:6. doi:10.1038/s43246-020-00104-z.

- [54] Makuła P, Pacia M, Macyk W. How To Correctly Determine the Band Gap Energy of Modified Semiconductor Photocatalysts Based on UV-Vis Spectra. *J Phys Chem Lett* 2018;9:6814–7. doi:10.1021/acs.jpcllett.8b02892.
- [55] Shannon RD. Revised effective ionic radii and systematic studies of interatomic distances in halides and chalcogenides. *Acta Crystallogr Sect A* 1976;32:751–67. doi:10.1107/S0567739476001551.
- [56] Gerling L, Mahato S, Voz C, Alcubilla R, Puigdollers J. Characterization of Transition Metal Oxide/Silicon Heterojunctions for Solar Cell Applications. *Appl Sci* 2015;5:695–705. doi:10.3390/app5040695.
- [57] Liu X, Gao J, Chen Y, Li C, Chen J, Qu W, et al. Rational Design of Alkali-Resistant NO Reduction Catalysts using a Stable Hexagonal V-Doped MoO₃ Support for Alkali Trapping. *ChemCatChem* 2018;10:3999–4003. doi:10.1002/cctc.201800818.